CFD PREDICTIONS OF NEAR-FIELD PRESSURE SIGNATURES OF A LOW-BOOM AIRCRAFT*

Kamran Fouladi
Lockheed Engineering & Sciences Company
Hampton, VA

Daniel Baize
NASA Langley Research Center
Hampton, VA

SUMMARY

A three dimensional Euler marching code has been utilized to predict near-field pressure signatures of an aircraft with low boom characteristics. Computations were extended to approximately six body lengths aft of the aircraft in order to obtain pressure data at three body lengths below the aircraft for a cruise Mach number of 1.6. The near-field pressure data were extrapolated to the ground using a Whitham based method. The distance below the aircraft where the pressure data are attained is defined in this paper as the "separation distance." The influences of separation distance and the still highly three-dimensional flow field on the predicted ground pressure signatures and boom loudness are presented in this paper.

INTRODUCTION

The existence of any future high speed civil transport (HSCT) aircraft will be governed largely by its environmental acceptability and economic viability. A major environmental concern of a high speed transport aircraft is the intense sonic boom it generates during supersonic flight. This concern has lead to international laws which prohibit overland supersonic commercial flights. However, the economic viability of proposed designs is drastically increased when supersonic cruise is maintained throughout the majority of the mission. Therefore, HSCT configurations with reduced sonic boom characteristics are very desirable, providing that the existing bans of overland supersonic flight could be affected. Accurate sonic boom predictions are

* Work done on contract at Lockheed Engineering & Sciences Company, NAS1-19000.

required before these regulatory changes and economic benefits can be pursued.

Traditional sonic boom prediction methods have been based on Whitham theory (Ref. 1), and its extension to wing bodies (Ref. 2). The effects of a stratified atmosphere were added to sonic boom predictions in Ref. 3. References 1, 2, and 3 predict sonic booms by the equivalent area method and they are referred to as "modified linear theory" methods. These prediction methods can be used reliably to predict sonic boom signatures on the ground from pressure signatures attained at a distance from the aircraft where three-dimensional and nonlinear effects have been significantly diminished. Other means of obtaining the near-field pressure signatures are wind tunnel testing and CFD calculations. The near-field pressure data can be extrapolated to the ground using methods such as those reported in Refs. 3-4. A sonic boom propagation method that included three-dimensional and nonlinear effects is presented in Refs. 5-7. However, extensive flow field data such as pressure, velocities, Mach numbers, flow angularities, etc., are required as input for that method which is based on the Method of Characteristics.

Although wind tunnel experiments were used exclusively to obtain near-field pressure data for Whitham based calculations in the past, recent improvements and maturation of numerical algorithms have made CFD methods a viable complement to experimental testing. In addition, the cost of model fabrication and wind tunnel operations continues to rise while the cost of high speed computing has dropped and its availability has significantly increased. Additionally, higher order CFD methods are now capable of simulating flows about complex configurations, such as HSCTs, with a high degree of accuracy (e.g. Refs. 8-11). Such methods can provide, for example, the extreme near-field and off-surface flow field information for aerodynamic analysis of an aircraft. It is also possible to predict the pressure signature several body lengths away. These signatures can then be extrapolated to the ground using modified linear theory. Off-flight track conditions may also be extracted, since the complete three dimensional solution about the aircraft is calculated.

In the past, it has been assumed that the loudest boom occurs on the centerline ground flight track, and the boom gets weaker as the distance from the centerline increases (Ref. 12). Thus, efforts concentrated on predicting and reducing the boom loudness on the flight path and sonic boom generated to the sides of the centerline were usually ignored. With the design of more sophisticated low boom configurations, there is a growing concern that these assumptions may no longer be valid. For example, the three dimensional results of Siclari and Darden (Ref. 10) have indicated that boom overpressures up to 40% greater in magnitude can be seen off-centerline for

the low boom aircraft considered in their study. This was attributed to shocks generated by aircraft's supersonic leading-edge wing crank.

Another issue of concern is the effect of "separation distance" on the ability to accurately predict ground pressure signatures and its associated loudness. Separation distance is defined herein as the distance below the aircraft where near-field pressure data are attained. The near-field pressure data are then extrapolated to the ground for sonic boom prediction using two-dimensional Whitham based methods. If the separation distance is too small, a pressure signature only in one plane may not contain all information necessary to assess the signature over the ground path. Conversely, due to constraints on computational resources, it is desirable to determine a minimum separation distance from the aircraft where nonlinear and three-dimensional effects are no longer prominent. A smaller computational domain is required for a smaller distance, thus significant savings in both computational time and memory can be obtained.

The objective of this paper is two fold: (i) predict the level of sonic boom generated both on- and off-centerline of flight path of a low boom configuration; (ii) investigate the effects of separation distance on the prediction of the ground sonic boom. Aerodynamic analysis and prediction of the near-field pressure signature of a newly designed low boom aircraft are performed using a three dimensional Euler code (Ref. 10) which has been recently modified for this purpose.

APPROACH

MIM3DSB (Multigrid Implicit Marching-Sonic Boom) is an Euler marching code specifically tailored for prediction of near-field pressure signatures of aircraft configurations (Ref. 10). The numerical scheme is based on a Jameson type explicit vertex based, finite volume method. The scheme initializes the flow field by a conical flow solution at the configuration apex. The three-dimensional solution is then computed using a hybrid implicit marching technique. MIM3DSB utilizes a central difference finite volume method in crossflow planes, and an implicit upwind finite difference technique in the marching direction to solve three-dimensional Euler equations on structured grids. A blend of second order and fourth order dissipation terms are added for stability and maintaining smooth shocks. Time integrations are performed using an explicit multistage Runge-Kutta technique. Local time stepping and residual smoothing are also utilized for convergence acceleration. Due to its marching nature, MIM3DSB is computationally

efficient and uses very little memory for large grids.

MIM3DSB has been used to predict sonic boom signatures of an axisymmetric projectile, and two low boom aircraft configurations (Refs. 10 and 11). Good correlation was achieved for the simple projectile. For low boom aircraft, the code was shown to achieve a good correlation with measured data for the forward half of the near-field signature. However, some discrepancies were observed in the latter half and they were attributed to possible deficiencies in the wind tunnel model and the numerical definition used (Ref. 10).

AIRCRAFT CONFIGURATION

The low boom configuration analyzed in this paper was designed to exhibit a "hybrid" sonic boom ground signature utilizing a combination of linear and modified linear methods. The "hybrid" signature type (Ref. 13) begins with a flat-top region which later converts to a ramp. This signature is thought to be less sensitive to atmospheric perturbations than the ramp type alone and illustrated in Fig. 1. The target ground signature for this concept has a nose overpressure of 0.84 psf for a cruise weight of 610,000 lbs at 47,000 ft. The ramp portion of the signature rises to an overpressure of 1.45 psf. The low boom aircraft is designed to transport 250 passengers over 5,500 nautical miles at a takeoff gross weight of 650,000 lbs. The cruise Mach number varies from Mach 1.6 overland (25% of cruise mission) to 2.0 over water (75% of cruise mission) where the signature is unconstrained. The aircraft is approximately 300 ft. long and has wing span of 140 ft. (Fig. 2).

COMPUTATIONAL GRID

Sonic boom computations require adequate grid resolution near the aircraft for aerodynamic analysis. Adequate resolution at several body lengths below and aft of the aircraft is also required for pressure signature predictions. A typical grid topology of crossflow plane grids stacked in the marching direction would not be suitable for such an application since the number of points normal to the body remains constant as the solution is marched downstream. This results in a very coarse mesh and loss of grid resolution and accuracy. To overcome this problem, Siclari and Darden (Ref. 10) proposed a unique multiblock grid topology. First, the base of configuration is extended with a sting of approximately one body length. The sting then expands into a Mach cone surface with the Mach angle of the freestream Mach number. A flow tangency boundary

condition is imposed on the surface of the aircraft and sting. A freestream boundary condition is applied on the surface of the Mach cone. The first block of the present grid topology, a series of crossflow plane grids stacked in the marching direction, contains the aircraft. The sting and the Mach cone surface are contained in the second block. The outer boundary of this grid topology is adapted to the shape of the bow wave by computation. Hence, each crossflow plane grid is extended in the normal direction to capture the bow and embedded shocks.The details of this procedure are given in Ref. 10.

The computational grid is generated internally by MIM3DSB and is shown in Fig. 3. Approximately 1.2 million grid points were used in this case. The resolution of the first block (Fig. 3a) is (89x64) in the crossflow planes with 100 marching steps. There are 112 axial steps in the second block (Fig. 3b) with (85x65) resolution in the crossflow planes. The computational time required for the present case on CRAY-YMP of NASA Langley Research Center is approximately 2 hours. The run time memory required is about 2.5 megawords, or 17 bytes per grid point.

RESULTS AND DISCUSSIONS

Computations were performed for the design overland cruise Mach number of $M_\infty = 1.6$ and cruise angle of attack, $\alpha = 3.84^\circ$. The computed pressure contours on the symmetry plane are illustrated in Fig. 4. The sting, which is about one aircraft length long, is also depicted in this figure. Flow field features such as shocks emanating from the nose, the wing leading and trailing-edges, and the sting attachment junction are captured and represented by isobars.

Figure 5 shows the pressure pattern in a plane perpendicular to the aft end of the aircraft. The bow shock and sting attachment shocks are also shown in this figure. The wing on the present model has a section with reduced sweep on the outer panels which generates a stronger shock that is illustrated in Fig. 5. Two axial stations were chosen to analyze the flow on the wing. In Fig. 6, Stations 1 and 2 are located immediately upstream and downstream of the leading-edge break point, respectively. A comparison of normalized pressure patterns at these stations (Fig. 6) shows a higher overpressure on the lower side of Station 2. An expansion region due to the contour of the fuselage is also shown at the upper side of Station 2.

To obtain the pressure signature on the ground at various azimuthal angles, flow fields on cylindrical surfaces at several radii were extracted from the three-dimensional solution. Three

cylinders with r/l= 0.5, 1.0, and 3.0 were chosen, where r/l is ratio of cylinder radius to length of the aircraft and is equivalent to the non-dimensional separation distance.

Figures 7-9 display the three-dimensional pressure footprint of the aircraft on these cylinders. Significant axial variation in the pressure pattern is featured on all cylinders. In addition, considerable circumferential variation is present on cylinders at r/l= 0.5 and 1.0. However, changes in circumferential pattern appear to have diminished at r/l = 3.0. Note that maximum and minimum pressures are represented by colors white and black, respectively, as indicated by the color bar.

Both on and off-centerline pressure signatures at a separation distance of r/l = 0.5 are illustrated in Fig. 10. The axial and circumferential variations can also be observed in the pressure signatures shown in these figures. Three distinct and separate overpressure peaks are evident for the lower azimuthal angles (e.g., $\Phi = 0°$ and 15°) at r/l = 0.5. The first peak represents the nose shock. The second and third peaks are attributed to the shocks emanating from wing leading-edge highly swept forward and reduced-sweep outer sections, respectively. The peaks are followed by an expansion and another shock due to the wing trailing-edge. At higher angles ($\Phi = 45°$) the leading-edge overpressure is mainly governed by the shock from the reduced sweep sections of the wing. Thus, the third peak becomes more prominent with an overpressure value greater than that of the third peak at lower angles. At r/l = 1.0 (Fig. 11), the centerline pressure signature becomes flat after the second peak and then ramps to the third peak. Off-centerline pressure signatures for this case display a behavior similar to that of r/l = 0.5. The pressure patterns at r/l= 3.0, shown in Fig. 12, indicate only two distinct overpressure peaks. It is assumed that the shocks due to wing leading-edge areas, before and after the leading-edge break point, have coalesced as they traveled three aircraft lengths.

The Thomas code (Ref. 5) was used to extrapolate the near-field pressure data to the ground. Pressure signatures on the ground are obtained by extrapolating near-field pressure signatures. The signatures at r/l = 0.5, 1.0, and 3.0 are used as inputs to the Thomas code. The flight altitude and ground reflection factor are assumed to be 47,000 and 1.9, respectively. The ground pressure signatures are plotted in Fig. 13. The signature at y = 0.0 is the signature on the flight track centerline and is extrapolated from the $\Phi = 0°$. Azimuthal angles of 15, 30, and 45 degrees result in lateral distances of y = 2.7, 6.0, and 12.0 miles, respectively.

For all azimuthal angles, the Thomas code predicts that the near-field signature would

persist to the ground. For example, the centerline ground pressure plot (Fig. 13a) displays signatures with the same overall features as observed in near-field. Figure 13a indicates that predicted initial rises on the ground due to nose overpressures have the same values for all three signatures and are approximately 0.9 psf. The magnitude of pressure rises due to the leading-edge on the ground decreases as the separation distance is increased. The magnitude of expansion and subsequent shock at the trailing-edge, however, increases with separation distance. Using propagation method of Ref. 5 and near-field pressure signatures from proper separation distances, it is expected to predict similar pressure signatures on the ground. However, comparison of the signatures plotted in Fig. 13a indicates that three noticeably different centerline pressure signatures from the same aircraft are predicted at the same location on the ground. The differences in these signatures are results of differences in the near-field signatures. That is perhaps the three-dimensional and nonlinear effects are still present and strong at smaller separation distances. Other factors resulting from smaller separation distances which may also affect the accuracy of extrapolated signatures are discussed by Mack and Darden (Ref. 14). Reference 14 discusses the need to determine limits on near-field separation distance at which pressure signatures are obtained for the purpose of extrapolation from the aircraft to the ground. At other lateral stations, the initial pressure rises for all three signatures have comparable but slightly smaller values than at the centerline (Fig. 13 b-d). Using Thomas code, it is predicted that the effects of atmosphere to be greatest at $\Phi = 45°$ (y = 12.0 miles). The leading-edge shocks appear to coalesce to one instantaneous shock. The magnitude of this shock also diminishes as separation distance is increased. An instantaneous shock from the trailing-edge is also evident in Fig. 13 d.

Figure 14 displays the ground pressure signatures at various azimuthal angles versus time. The signatures are extrapolated from the near-field pressure data calculated at r/l = 0.5. The three-dimensional effects of the aircraft are clearly shown in this figure. The largest initial pressure rise occurs at the centerline. However, the secondary shock appears to be greatest at y=12.0 miles.

Although the extrapolated signatures exhibit some similar features, they produce different levels of loudness on the ground. The loudness of each signature is calculated following a procedure proposed by Shepherd and Sullivan (Ref. 15) and is plotted versus the lateral distance to the side of the flight path axis (y) in Fig. 15. Loudness is a well-understood characteristic of human hearing and provides a reasonable prediction of people's reaction to sonic booms (Refs. 15 and 16). Loudness can be used as a parameter to quantify the magnitude of sonic booms. Therefore, it is suitable for comparative assessments of different ground pressure signatures.

The aircraft's three-dimensional effects on the loudness are illustrated in Fig. 15. For all separation distances, the loudest boom is felt on centerline. This is expected since the initial pressure jump at each separation distance is shown to be greatest at the centerline (Fig. 14). However, the loudness does not continually decrease as lateral distance is increased from the centerline. For example, for a signature from r/l = 3.0, the magnitude of loudness at y =12.0 miles is about 0.5 dB(PL) greater than the loudness magnitude at y = 2.7 and 1.7 dB(PL) greater than at 6.0 miles, respectively. This is consistent with the fact that the loudness prediction procedure takes the entire waveform into consideration and larger values of the intermediate shocks are observed at $\Phi = 45°$. The near-field pressure signatures of angles greater than 50° are not predicted to reach the ground. Signatures from r/l = 0.5 and 1.0 exhibit similar loudness behavior.

The shock coalescence and flow smoothing that take place further away from the aircraft will result in diminishing the nonlinear and three-dimensional effects. Therefore, the level of loudness on the ground should be independent of separation distance, if pressure data are taken from proper separation distances. The effects of separation distances which are considered here are summarized in Fig. 15. The level of loudness generated by a signature decreases as the starting solution separation distance increases. This is due to the fact that different ground pressure signatures were predicted from near-field pressure signatures at various separation distances (Fig. 13). Additionally, it is important to note that in order to obtain the pressure data at about three body lengths below the aircraft in the present study, the computation must be carried out to about five to six body lengths aft of the aircraft. Hence, larger grid step sizes in the axial direction are required for this extended computation. Therefore, there are possibilities of shock smearing and inherent inaccuracies due to large step sizes which may affect the solutions at larger separation distances. Further grid refinement study in the axial direction may indicate to what extent the differences in the levels of loudness for signatures from different separation distances are attributed to grid sensitivity.

CONCLUSIONS

Flow past an aircraft with low boom characteristics was computationally simulated. This was accomplished by solving the three-dimensional Euler equations on an efficient structured grid tailored for sonic boom calculations. The near-field pressure signatures both on and off-axis at three separation distances below the aircraft were obtained.

The influence of separation distance on the near-field pressure patterns, predicted ground pressure signatures, and the level of loudness on the ground was shown. The pressure data from all three distances produced signatures with similar overall features and yet different levels of loudness. These differences were attributed to diminishing nonlinear and three-dimensional effects that take place further away from the aircraft. Loss of grid resolution due to large grid step sizes may also contribute to this cause. In summary, the level of loudness decreased as the separation distance was increased. Future work will involve a grid refinement study to investigate the effects of grid resolution on the predicted level of loudness on the ground.

The pressure patterns on cylindrical surfaces were obtained to investigate the three-dimensional effects of the aircraft on the sonic boom patterns. These effects were presented via ground pressure signatures and boom loudness. The largest initial rise in the pressure was observed at the centerline and that resulted in the loudest boom predicted on the flight track axis. However, loudness of similar magnitude may be felt at about 12.0 miles to the sides of the centerline where larger intermediate shocks with smaller rise times were predicted.

REFERENCES

1. Whitham, G.: The Flow Pattern of a Supersonic Projectile. Commun. Pure & Applied Math.
2. Walkden, F.: The Shock Pattern of a Wing-Body Combination, Far From the Flight Path. Aeronautical Q., Vol. IX, Pt. 2, May 1958, pp 164-194.
3. Hayes, W, Haefeli, R., and Kulsrud, H.: Sonic Boom Propagation in a Stratified Atmosphere, with a Computer Program. NASA CR-1299, 1969.
4. Thomas C.: Extrapolation of Sonic Boom Pressure Signature by the Waveform Parameter Method. NASA TN D-6832, June 1972.
5. Ferri, A., Siclari, M., Ting, L.: Sonic Boom Analysis for High Altitude Flight at High Mach Numbers. AIAA Paper No. 73-1035, October 1973.
6. Ferri A., Ting, L., and Lo, R.: Nonlinear Sonic Boom Propagation Including the Asymmetric Effects. AIAA J., Vol. 15, No. 5, May 1977, pp 653-658.
7. Darden, C.: An Analysis of Shock Coalescence Including Three-Dimensional Effects

8. Vatsa, V., Turkel, E., and Abolhassani, J.: Extension of Multigrid Methodology to Supersonic/Hypersonic 3-D Viscous Flow. NASA CR-187612, August 1991.

9. Pittman, J., Bonhaus, D., and Siclari, M.: Euler Analysis of a High Speed Civil Transport Concept at Mach 3. J. of Aircraft, Vol. 28, No. 4, April 1991, pp 239-245.

10. Siclari, M. and Darden, C.: CFD Predictions of the Near-Field Sonic Boom Environment for Two Low Boom HSCT Configurations. AIAA Paper No. 91-1631, June 1991, Honolulu, Hawaii.

11. Siclari, M. and Darden, C.: An Euler Code Prediction of Near- to Mid-Field Sonic Boom Pressure Signature. AIAA Paper No. 90-4000, Oct. 1990, Tallahassee, Florida.

12. Darden, C., Hayes, W., George, A., and Pierce A.: Status of Sonic Boom Methodology and Understanding. NASA CP-3027, January 1988, Hampton, Virginia.

13. Haglund, G.: HSCT Designs for Reduced Sonic Boom. AIAA Paper No. 91-3130-CP, September 1991, Baltimore, Maryland.

14. Mack, R. and Darden, C.: Limitations on Wind-Tunnel Pressure Signature Extrapolation. Sonic Boom Workshop, NASA CP-3173, 1992.

15. Shepherd, K. and Sullivan, B.: A Loudness Calculation Procedure Applied to Shaped Sonic Booms. NASA TP-3134, November 1991.

16. Darden, C., Shepherd, K.: Assessment and Design of Low Boom Configurations for Supersonic Transport Aircraft. DGLR/AIAA 14th Aeroacoustic Conference, Aachen, Germany, May 1992.

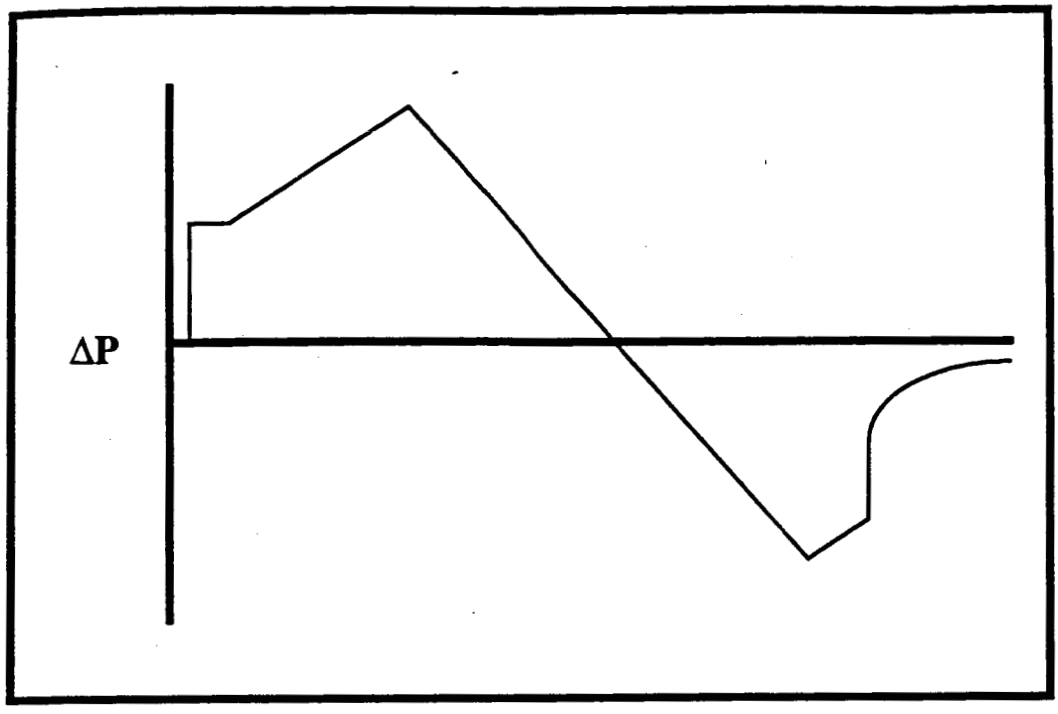

Figure 1. A "hybrid" sonic boom signature, flat top and ramp.

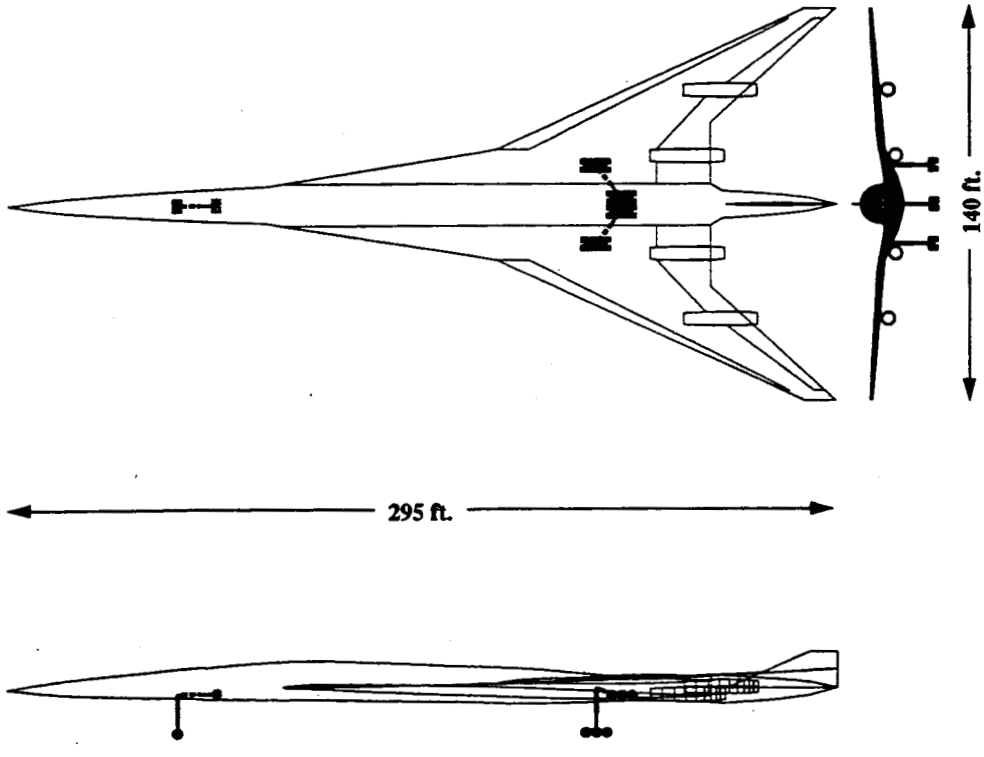

Figure 2. Geometry of the low boom aircraft.

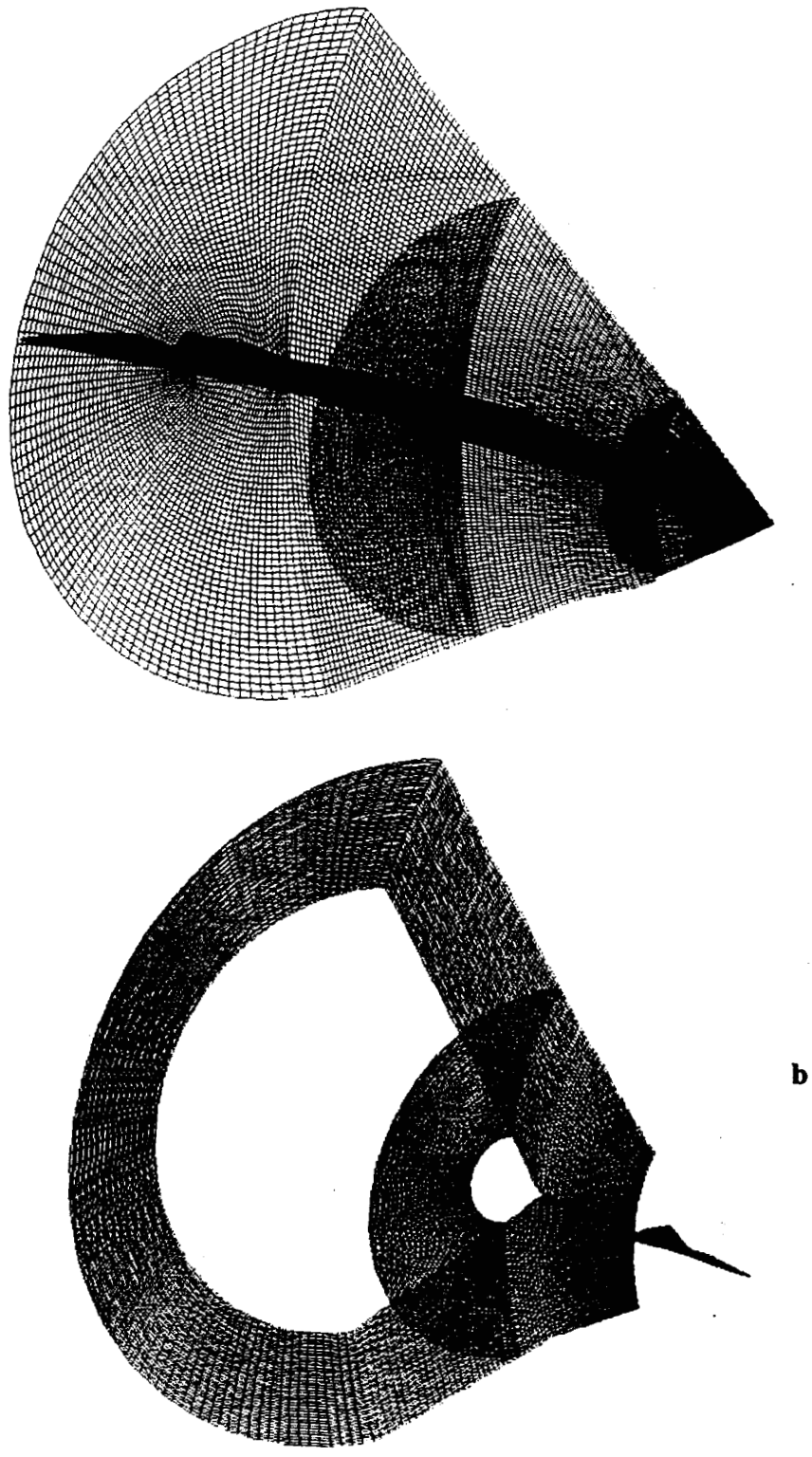

Figure 3. Two-block grid topology of sonic boom computation, a) Block 1, b) Block 2.

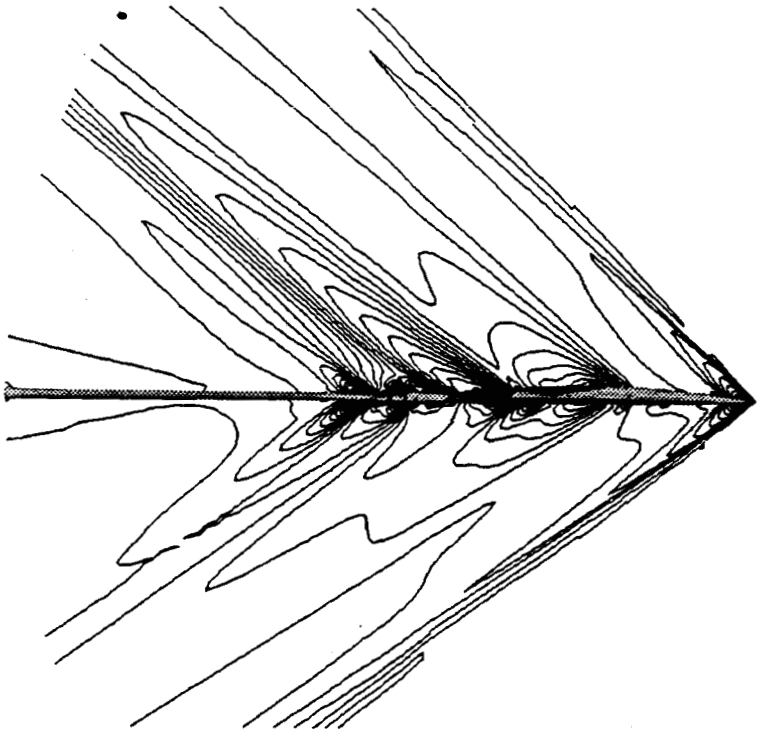

Figure 4. Computed pressure contours on the plane of symmetry.

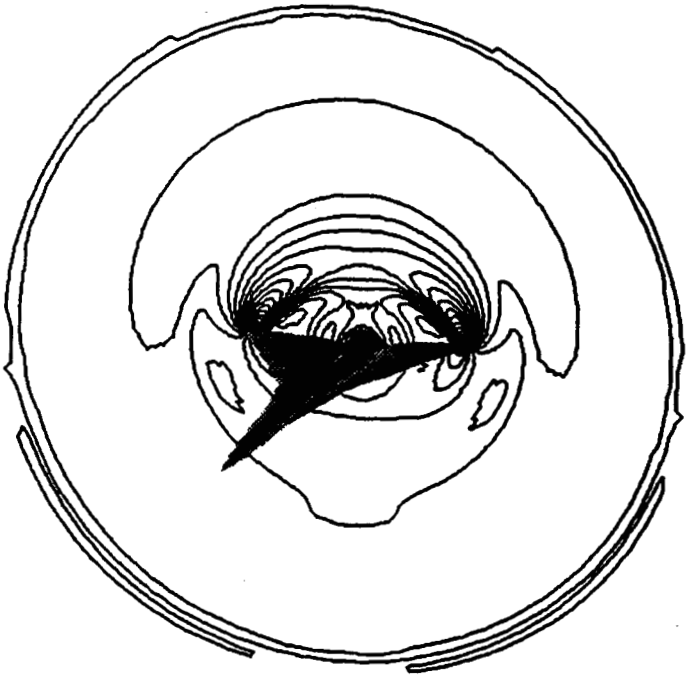

Figure 5. Computed pressure pattern at the aft end of the aircraft.

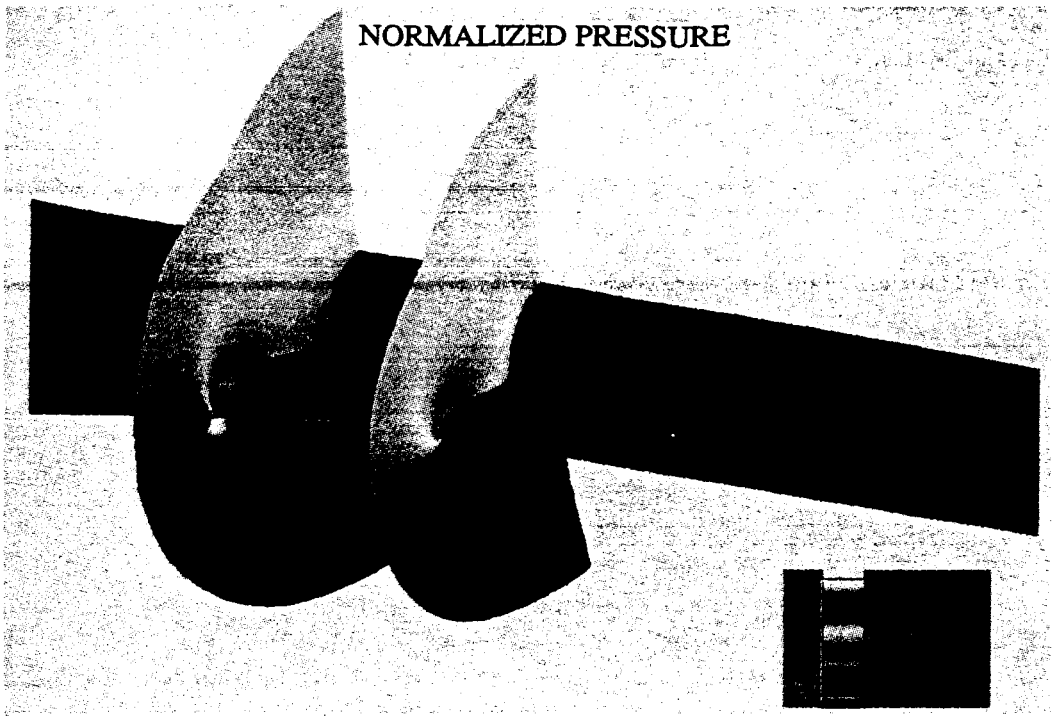

Figure 6. Computed crossflow pressure patterns on the wing at two axial stations.

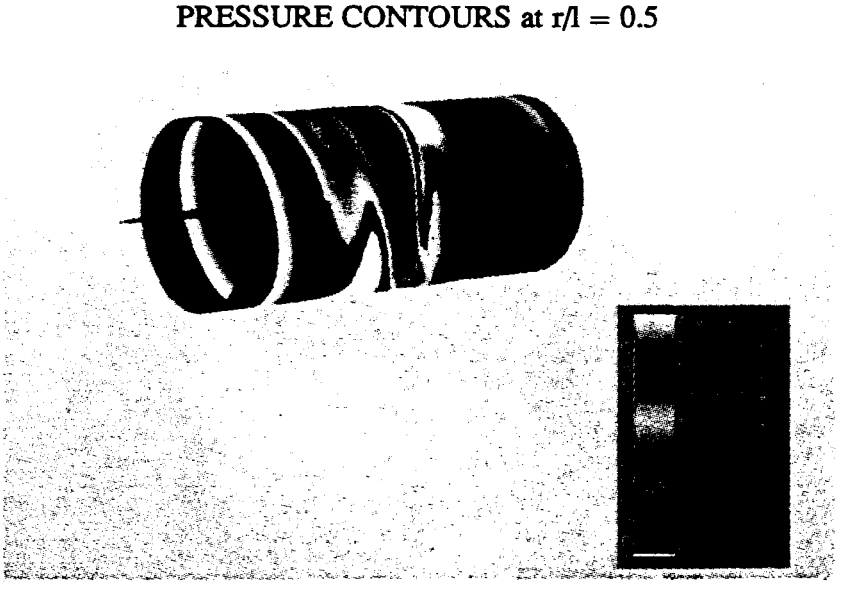

Figure 7. Three-dimensional pressure footprint of the aircraft on a cylindrical surface with r/l = 0.5.

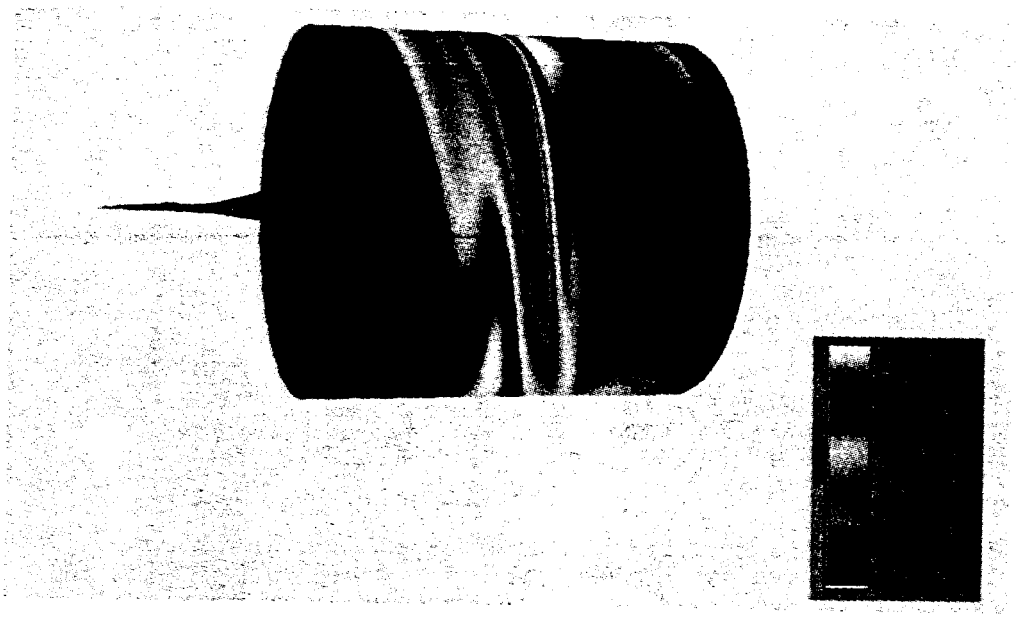

Figure 8.Three-dimensional pressure footprint of the aircraft on a cylindrical surface with r/l = 1.0.

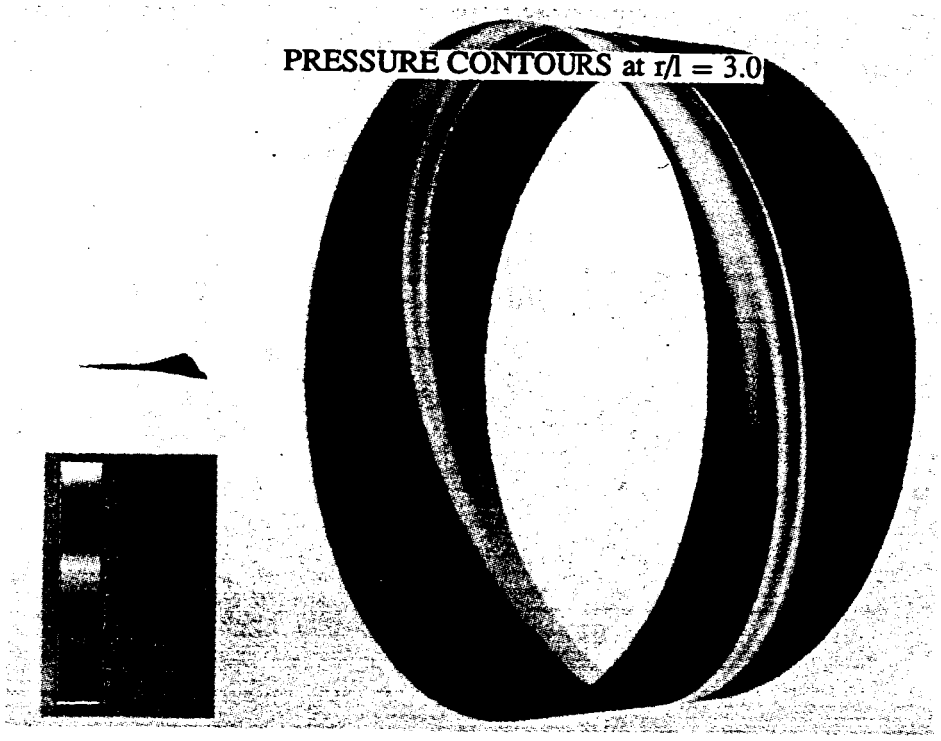

Figure 9. Three-dimensional pressure footprint of the aircraft on a cylindrical surface with r/l = 3.0.

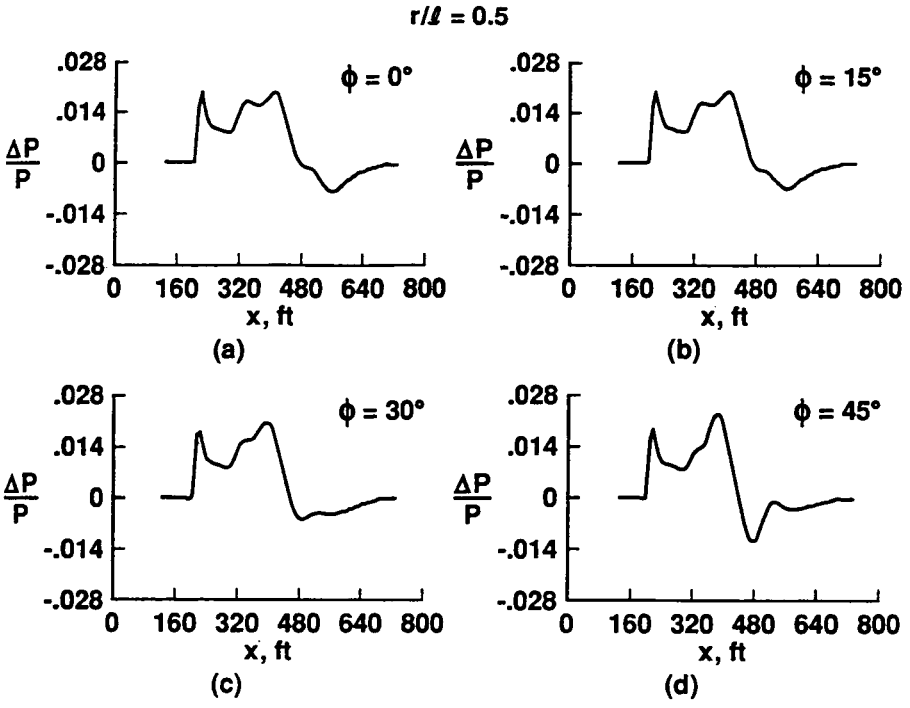

Figure 10. On and off-centerline pressure signatures at r/l = 0.5.

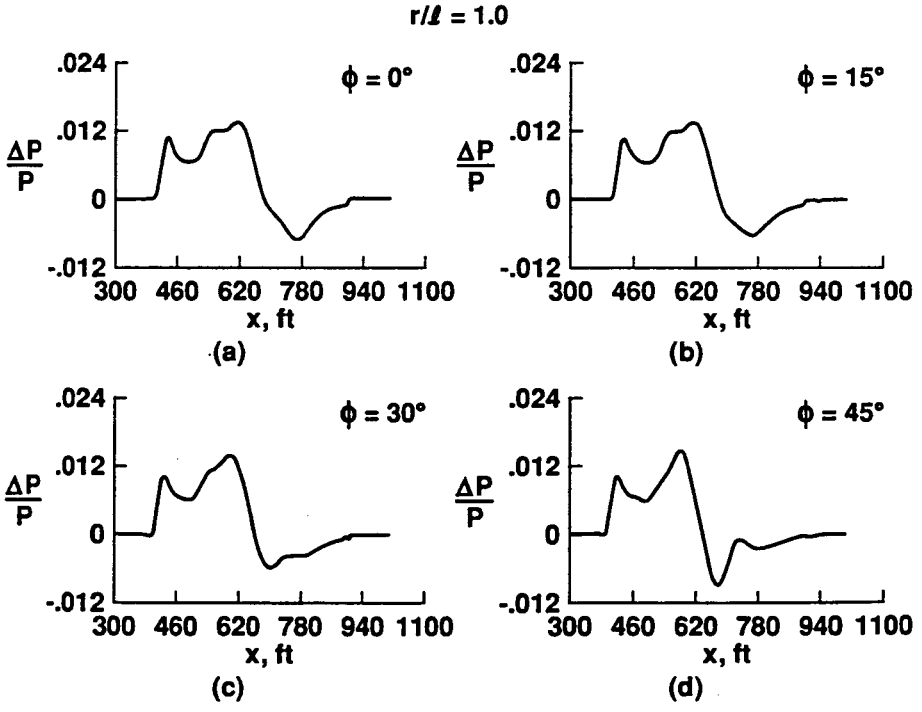

Figure 11. On and off-centerline pressure signatures at r/l = 1.0.

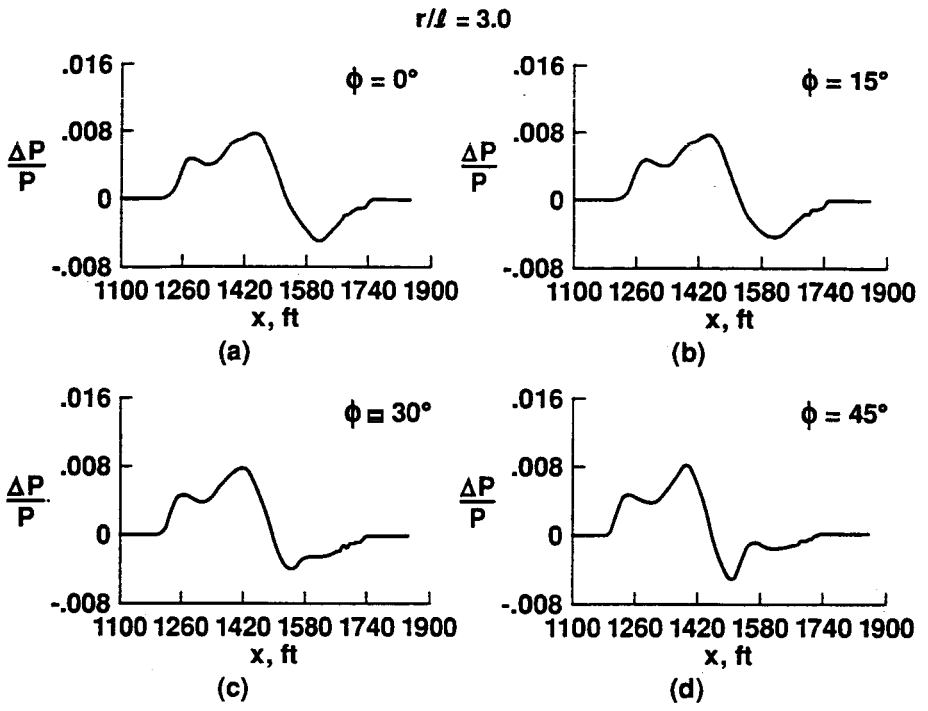

Figure 12. On and off-centerline pressure signatures at r/l = 3.0.

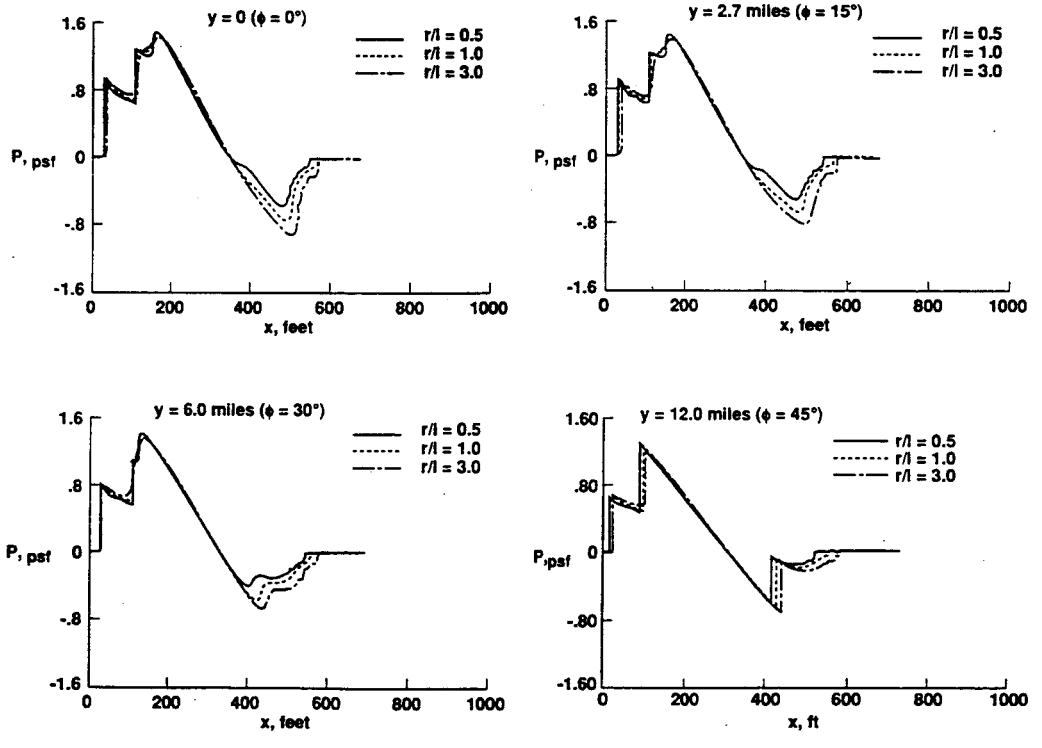

Figure 13. Predicted ground pressure signatures.

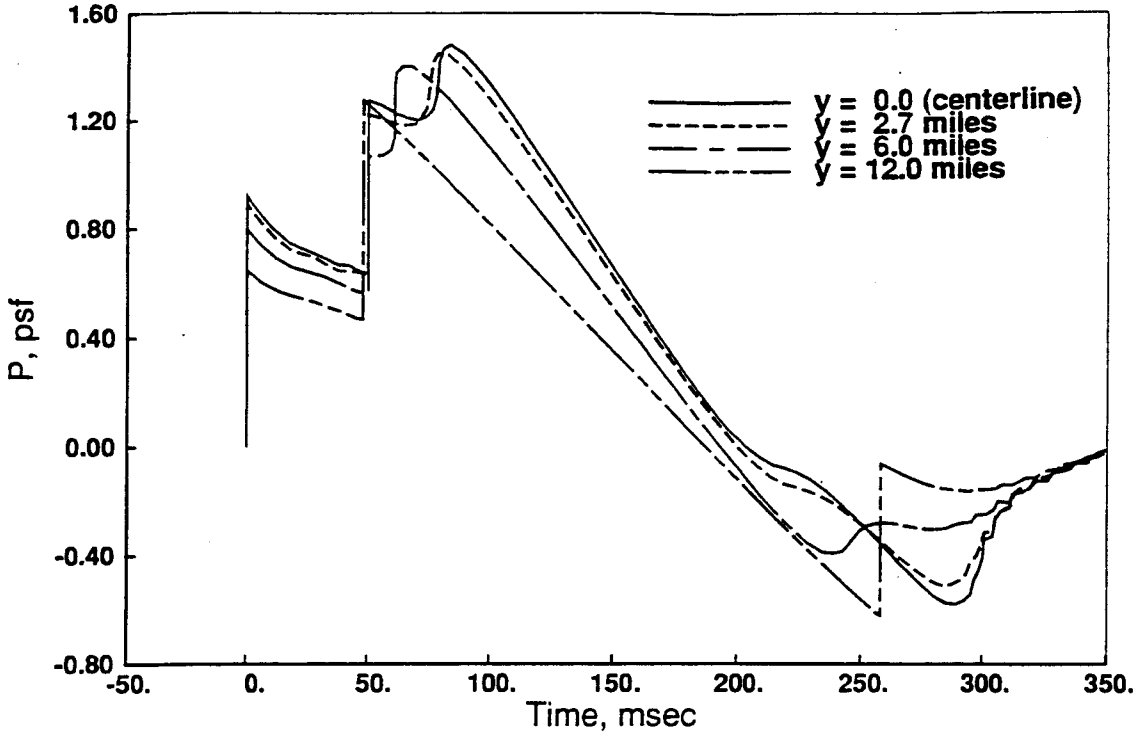

Figure 14. Predicted ground pressure signature at various lateral stations extrapolated from r/l = 0.5.

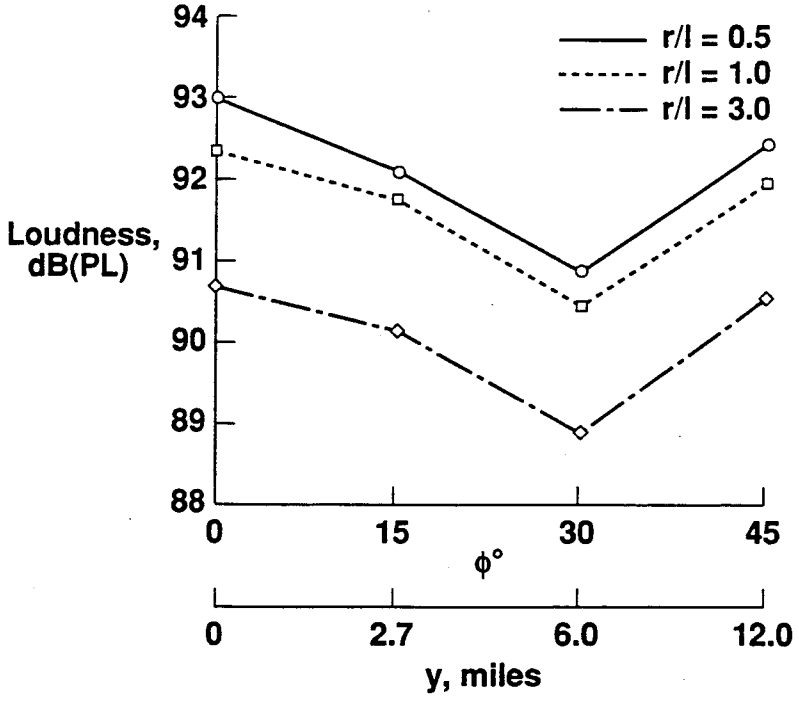

Figure 15. Three-dimensional and separation distance loudness trends.